Development of a Control Strategy for the Hybrid Energy Storage Systems in Standalone Microgrid

Hocine Guentri

Abdelhafid Boussouf University centre of Mila,
Mila, Algeria
Department of Mechanic and Electromechanics,
Institute of Science and Technologies,
GE Laboratory, Saida
Mila city, Algeria
hguentri2005@centre-univ-mila.dz

Abdeldjalil Dahbi

Unité de Recherche en Energies Renouvelables
en Milieu Saharien(URERMS), Centre de
Développement des Energies renouvelables(CDER),
01000, Adrar, Algeria
Laboratory of sustainable Development and
informatics, (L.D.D.I), University of Adrar
Adrar city, Algeria
dahbi_j@yahoo.fr

Tayeb Allaoui

Ibn Khaldoun university of TIARET,
Department of Electrical Engineering, Faculty of
Applied Science, L2GEGI Laboratory
Tiaret, Algeria
allaoui_tb@yahoo.fr

Salim Aoulmit

Abdelhafid Boussouf University centre of Mila,
Department of Mechanic and Electromechanics,
Institute of Science and Technologies,
Mila, Algeria
s.aoulmit@centre-univ-mila.dz

Ahmed Bouraiou

Unité de Recherche en Energies Renouvelables
en Milieu Saharien(URERMS), Centre de
Développement des Energies renouvelables(CDER),
01000, Adrar, Algeria
Laboratory of sustainable Development and
informatics, (L.D.D.I), University of Adrar
Adrar, Algeria
bouraiouahmed@gmail.com

Abstract – *The intermediate energy storage system is very necessary for the standalone multi-source renewable energy system to increase stability, reliability of supply, and power quality. Among the most practical energy storage solutions is combining supercapacitors and chemical batteries. However, the major problem in this kind of application is the design of the power management, as well as the control scheme of hybrid energy storage systems. The focal purpose of this paper is to develop a novel approach to control DC bus voltage based on the reference power's frequency decomposition. This paper uses a storage system combined of batteries and supercapacitors. These later are integrated in the multi-source renewable energy system to supply an AC load. This technique uses the low-pass filters' properties to control the DC bus voltage by balancing the generated green power and the fluctuating load. The hybrid storage system regulates power fluctuations by absorbing surplus power and providing required power. The results show good performances of the proposed control scheme, such as low battery current charge/discharge rates, lower current stress level on batteries, voltage control improvements, which lead to increase the battery life.*

Keywords: *Photovoltaic, wind turbine generator, energy management, batteries, supercapacitor, hybrid energy storage*

1. INTRODUCTION

Renewable energies become a very promote solution against environment problems and a suitable drawback for remote area. However, the intermittence criteria of these sources make the Standalone Multi-source Renewable Energy Generation Systems (SMREGS) necessitate an intermediate energy storage system (ESS) to improve their stability, power quality, and supply reliability [1]. Chemical batteries, particularly lead-acid and lithium-ion batteries, are the most often utilized energy storage systems due to their high energy density and low cost relatively [1].

However, the primary drawbacks of these batteries are their limited lifespan and performance degradation in deep draining and overcharging cases. In order to enhance the capability and flexibility of the ESS, the combination of two or more energy storage technologies is a good solution in a hybrid configuration (HESS) [2].

Recently, researchers have shown increasing interest in investigating HESS and its applications. The most effective HESS configuration many researchers propose is the combination of chemical batteries with supercapacitors (SCs). Despite of SCs have a high power density, their energy density is relatively low [3]. They have a higher life cycle than batteries; they can also be charged and discharged quickly. Since each ESS has its drawbacks, the combining between the high density of the battery and the quick SC charging and discharging improves the overall reliability of the ESS.

However, the major problem with this kind of application is how to design the power management and control scheme of HESSs consisting of batteries and SCs [4]. Different control and management strategies have been proposed in the literature to stabilize the DC bus voltage and maintain a stable battery current during the transient time. Battery activities should be monitored and managed to operate safely continuously [5]. The most common techniques depend on a low-pass filter's frequency decomposition of the reference value, as proposed in [6, [7], or a discrete wavelet transform, as presented in [8, [9]. Other proposed model of predictive control-based methods, such as artificial neural networks [10], fuzzy supervisory control [11], and fuzzy adaptive control [12]. Authors in [13] used a genetic algorithm-based fuzzy logic controller to optimize the HESS. In [14], the adaptive power management of a standalone hybrid renewable energy system has been presented. In [15], the authors design an efficient energy management structure to improve the control of the HESS, which consists of batteries and supercapacitors. Also, in [16], the authors propose and develop the idea of using a community supercapacitor in an islanded DC multiple nano-grids system. In addition, in [17] the authors used only a PV source to provide electrical energy to a DC load, where the control strategy was based on the DC bus voltage regulation. However, in the current paper a hybrid system consisted of two sources (PV and wind) have been used, to supply an AC load via an inverter. Whereas, the control strategy is bases on the power regulation. The primary goal of this study is to develop a novel DC bus voltage management method based on the frequency decomposition of the reference power and a low-pass filter for the production of renewable energy from multiple sources. These sources supply an AC load with the help of a hybrid storage system composed of batteries and supercapacitors to improve the ESS and the stability of the DC bus voltage, power quality, and supply reliability.

The paper is organized as follows: Section 2 describes the system and the modeling of the different components. Section 3 presents the proposed energy management and control strategy of the HESS. Simulation results will be presented and discussed in Section 4. Finally, Section 5 summarizes this work's conclusions.

2. SYSTEM DESCRIPTION AND MODELING

The proposed renewable energy power system includes a wind turbine, a photovoltaic panel, and an ESS combining lithium batteries with an SC. As shown in Figure 1, all components are connected to a DC bus via a power converter. The whole system is connected to the AC load using a DC-AC converter.
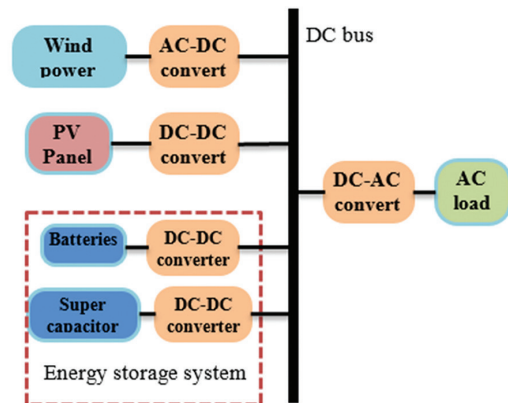
Fig. 1. Hybrid power system model

2.1. MODELING OF THE WIND ENERGY SYSTEM

The Wind Energy System is based on a permanent magnet synchronous generator (PMSG) coupled to the DC bus through a controlled AC-DC converter, it operates on variable speed mode with the pitch angle control as illustrated in Fig. 2 [18].
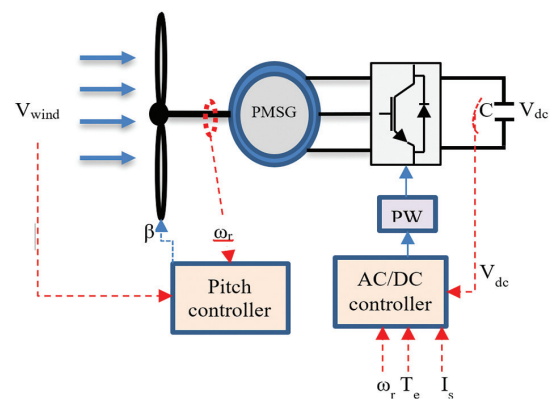
Fig. 2. Wind energy system configuration

2.1.1. Wind turbine model

The mechanical power produced by the wind turbine may be expressed as [19]:

$$P_m = \frac{1}{2}\rho\pi R^2 V_w^3 C_p(\lambda, \beta) \tag{1}$$

where P_m is the captured wind power (W), ρ is the air density (Kg/m³), R is the blade radius (m), V_w is the wind

speed (m/s), and C_p is the power coefficient. Based on the wind turbine characteristics, the value of C_p depends on the tip speed ratio (λ) and blade pitch angle (β) as:

$$C_p(\lambda,\beta) = c_1\left(\frac{c_2}{\lambda_i} - c_3\beta - c_4\right)e^{\frac{c_5}{\lambda_i}} + c_6\lambda \qquad (2)$$

$$\frac{1}{\lambda_i} = \frac{1}{\lambda - 0.08\beta} - \frac{0.035}{\beta^3 + 1} \qquad (3)$$

$$\lambda = \frac{\omega_r R}{V_w} \qquad (4)$$

where c_1 to c_6 as given in Table 1, they denote the characteristic coefficients of the wind turbine.

Table 1. Wind turbine coefficients characteristics

c_1	c_2	c_3	c_4	c_5	c_6
0.5176	116	0.4	5	21	0.0068

2.1.2. The permanent magnet synchronous generator (PMSG) modeling

The stator voltage of the three-phase PMSG using the two-phase orthogonal rotating dq reference frame based on Park transformation is given by: [20, 21]:

$$\begin{cases} V_{ds} = I_{ds}R_s + L_{ds}\dfrac{dI_{ds}}{dt} - \omega_e L_{qs}I_{qs} \\ V_{qs} = I_{qs}R_s + L_{qs}\dfrac{dI_{qs}}{dt} + \omega_e(L_{ds}I_{ds} + \lambda_{pm}) \end{cases} \qquad (5)$$

$$T_{em} = \frac{3Np}{4}(I_{qs}\lambda_{pm} - I_{ds}I_{qs}(L_{ds} - L_{qs})) \qquad (6)$$

where L_{ds}, L_{qs} are the inductances in d and q axis, I_{ds}, I_{qs}, V_{ds}, V_{qs} represent respectively currents and voltages in d and q axis, R_s is the stator resistance, ω_e denotes the electric angular frequency, λ_{pm} is the permanent magnet flux, p is the number of pole pairs.

The PMSG electrical scheme in dq reference frame is shown in Fig. 3.
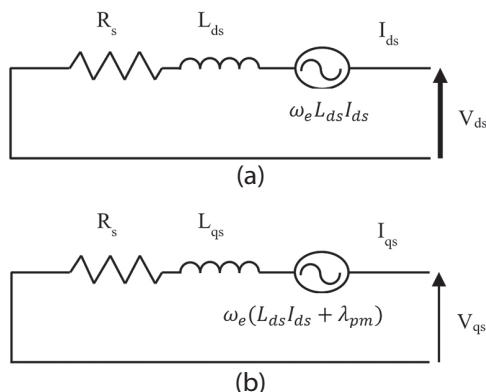
Fig. 3. PMSG (a) d-axis (b) q-axis circuit diagram

2.2. MODELING OF THE PHOTOVOLTAIC POWER GENERATOR

The photovoltaic (PV) system consists of a PV panel and a DC-DC boost converter controlled using the perturb and observe Maximum Power Point Tracking (MPPT) technique as shown in Fig. 4. The DC-DC converter's function is used to modify the impedance to provide the optimum energy from the PV panel [22].
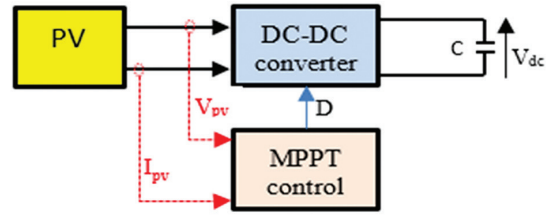
Fig. 4. Scheme of the photovoltaic system

Fig. 5 shows the commonly used model for a solar cell. It includes a photocurrent, a diode, a series resistor representing internal resistance to the passage of the current, and a parallel resistor representing the leakage current [23].
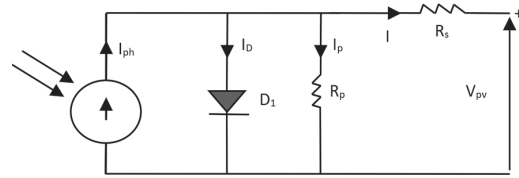
Fig. 5. PV cell equivalent circuit model

The equation of voltage-current characteristics of a solar cell's can be expressed by:

$$I = I_{ph} - I_s\left[exp\left(\left(\frac{qV + IR_s}{kT_cA}\right) - 1\right) - \left(\frac{V + IR_s}{R_p}\right)\right] \qquad (7)$$

where I_{ph} is a photocurrent, I_s is the cell saturation of dark current, q is the electron charge (q=1.6.10-19C), the Boltzman's constant (k=1.3.10-23 J/K), T_c is the cell's working temperature (Kalvin), and A is the ideality factor.

Equation (8) define the saturation current I_s as following:

$$I_s = I_p\left(\frac{T_c}{T_{ref}}\right)^3 exp\left(qG_r\left(\frac{1}{T_{ref}} - \frac{1}{T_c}\right)\cdot\frac{1}{kA}\right) \qquad (8)$$

where T_{ref} is the cell's reference temperature, and G_r is the solar irradiance.

The PV array comprises many PV modules that are electrically coupled in both parallel and serial circuits in order to produce the necessary current and voltage. With N_p, N_{sare} respectively number of parallels and series modules, the output or load current is calculated as [24]:

$$I = N_pI_{ph} - N_pI_s\left[exp\left(q\left(\frac{V}{N_s} + \frac{IR_s}{N_p}\right)\frac{1}{kT_cA}\right) - 1 - \left(\frac{N_pV}{N_s} + IR_s\right)\frac{1}{R_p}\right] \qquad (9)$$

2.3. MODELING OF THE BATTERIES

Battery modeling involves two steps: (1) the choice of a suitable model structure, (2) the determination of the model's parameter values. The RC ladder circuit shown in Fig. 6 is adopted in this research, because of

its excellent modeling accuracy and low computational complexity [25].

It is assumed that all cells are identical and the battery performance is unaffected by the packaging components. The connection of the cells (in series and parallel) does not affect the parameter values of the pack model. The battery pack connected in n-series has a fixed capacity. The battery pack model's open-circuit voltage (OCV) and R_s are computed as n times of the cell's R_s and OCV [6].

$$V_{bat} = OCV + \left(R_s + \sum_{i=1}^{n} Z_i \right) I_t \qquad (10)$$

$$Z_i = R_i + \frac{1}{jC_i\omega} \qquad (11)$$
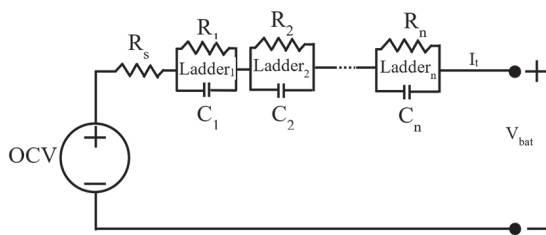
Fig. 6. The second RC ladder model structure

2.4. MODELING OF THE SUPERCAPACITORS

Various models of SC's have been reported in the literature based on their dynamic behaviour. The elementary series R-C is used in this work because of its simplicity and ability to replicate the actual SC's dynamic behaviour accurately. In [26], it is shown that SCs exhibit non-integer (fractional) behaviour and have a fractional impedance which is composed of a series resistor R_s and a fractional-order capacitor C_λ, as it is shown in Fig. 7.
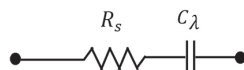
Fig. 7. Supercapacitors fractional series R-C model

The R-C series SC model's total equivalent impedance can be described as:

$$Z(s) = R_s + \frac{1}{C_\lambda S^\lambda} \qquad (12)$$

Where C_λ is the pseudo-capacitance with order λ ($0 \le \lambda \le 1$).

3. ENERGY MANAGEMENT AND CONTROL STRATEGIES

The control strategy aims to accomplish the power flow of the HESS to reach the following main goals: (1) decreasing of dynamic battery stress levels; (2) maintaining a stable DC voltage; (3) avoiding deep discharge of the battery; and (4) improving the system's overall efficiency.

The HESS shown in Fig. 8 presents the combination of batteries with supercapacitors. Each storage device is coupled to the DC bus via a bidirectional buck-boost converter. HESS is used to preserve the constant DC bus voltage (V_{dc}) because of the imbalance between demand and multisource generation. If the multisource generation is lower than demand, the DC bus voltage V_{dc} decreases from its reference value. HESS would then discharge to satisfy the excess demand. Likewise, if the multisource generation exceeds the demand, the DC bus voltage increases from its reference value. As a result, HESS will charge to consume the extra power.

The block diagram of the control approach is shown in Fig. 9. The control allows batteries to support slow transients in the long term, whereas the SC supports fast transients in a short time [9].
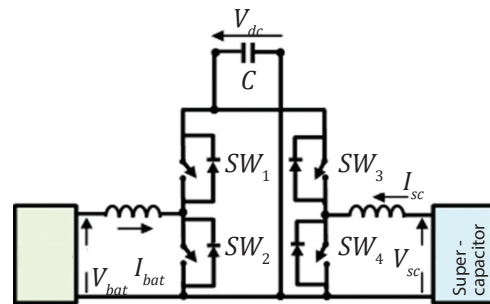
Fig. 8. HESS system
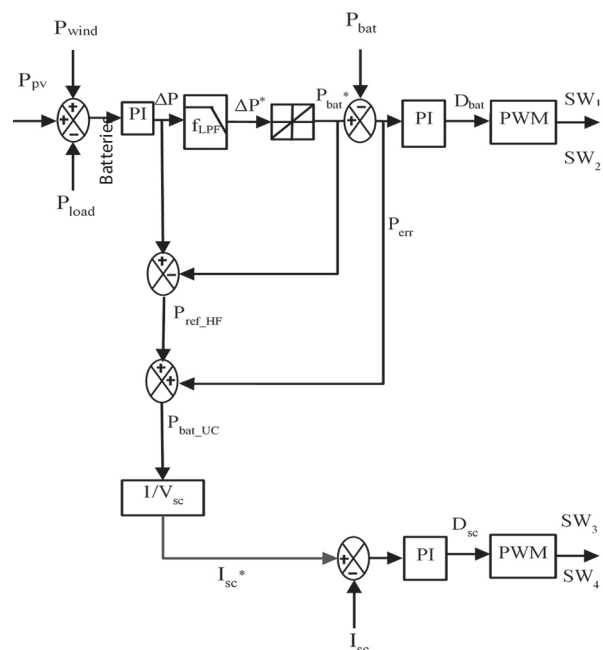
Fig. 9. The block diagram of the control strategy

The power deficit between the load demand and the generation from several sources, which is the total power that must be delivered by the HESS, it is given by:

$$\Delta P = P_{pv} + P_{wind} - P_{load} = P_{bat} + P_{sc} \qquad (13)$$

Therefore, the ΔP value includes the high-frequency element, which the SC provides. However, batteries provide the low-frequency components.

In this work, a low pass filter has been proposed to determine the low-frequency element, which represents the deficit reference power, as given:

$$\Delta P^* = f_{LPF}(\Delta P) \tag{14}$$

Where, f_{LPF} is the low-pass filter function. The charge limiter is used to deliver batteries' reference power, which is provided by [27]:

$$P_{bat}^* = f_{LPF}(\Delta P^*) \tag{15}$$

The real value (P_{bat}) is compared with this reference. The PI controller receives the error to generate the duty cycle D_{bat} to adjust the PWM control signal for battery converter switches (SW1 and SW2), as seen in Fig. 9.

Furthermore, the high frequency component (P_{ref_HF}) is deduced as following.

$$P_{ref\_HF} = \Delta P - P_{bat}^* \tag{16}$$

Therefore, the uncompensated battery power is:

$$P_{bat\_UC} = P_{ref\_HF} + P_{err} \tag{17}$$

The SC will supply the uncompensated battery power. As a result, the SC reference current will be:

$$I_{sc}^* = \frac{P_{bat\_UC}}{V_{sc}} \tag{18}$$

A similar control strategy is applied to SC. The PI controller will produce the duty cycle Dsc to generate the PWM signal for the SW3 and SW4 supercapacitor converter switches, as seen in Fig. 9.

4. SIMULATION AND RESULTS

The complete model of the system described in Figure 1 has been simulated in a MATLAB/Simulink environment under various operation conditions to evaluate the performance of the proposed control and management strategy.

Table 2 (Appendix) lists the model parameters utilized in this simulation investigation. Where K_{p_v}, K_{p_bat}, K_{p_sc} are the proportional gains for the DC bus voltage, batteries, and supercapacitor PI controllers, respectively, and K_{i_v}, K_{i_bat}, K_{i_sc} are the integral gains of the DC bus voltage, batteries and supercapacitor PI controllers, respectively.

The batteries and supercapacitor are assumed to be initially charged. The simulations are performed under different operating conditions, including variable irradiance, variable wind speed, and variable load.

Case: 1 Variable solar irradiation, constant wind speed and constant load

The solar irradiation profile employed in this simulation scenario is shown in Fig. 10, whereas the wind speed and load are fixed.

The performance of the proposed management and control strategy under variable solar irradiation is shown in Fig. 11 and 12. The load requests always 19 kW, as seen from (0 s to 1 s): P_{pv} =10 kW, the wind power provides about

4.9 kW, while the battery supplies the remaining power. Similarly, the battery power follows the PV power variations. The battery is in discharge mode, providing insufficient power until reaching the load power request (19 kW). Alternatively, when there is an excess of power, the battery is in charging mode and stores the extra energy.
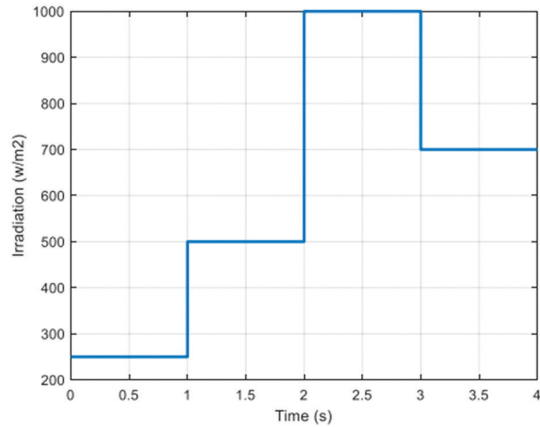
Fig. 10. Solar irradiance
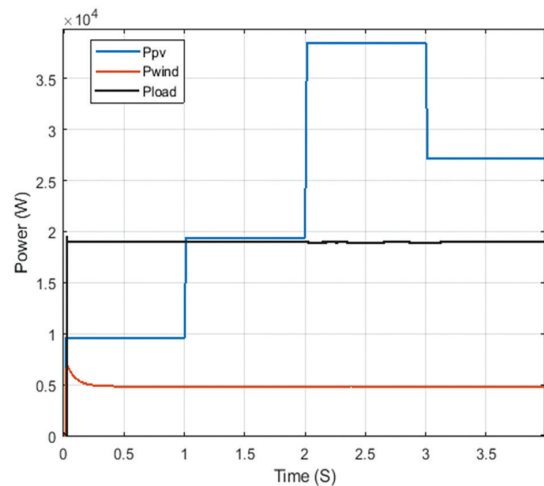
Fig. 11. Simulation of P_{pv}, P_{wind} and P_{load} with variable solar irradiance
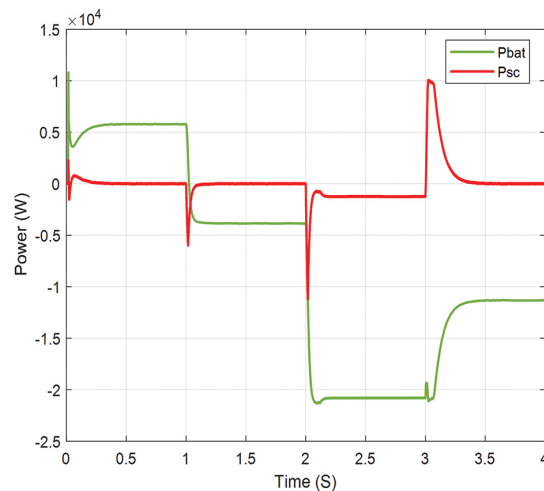
Fig. 12. Simulation of P_{pv}, P_{wind} and P_{load} with variable solar irradiance

Case: 2 Variable wind speed with a constant solar irradiation and constant load.

Fig. 13 illustrates the wind speed profile used in this simulation scenario. In this case, the solar irradiance and loads are kept constant.
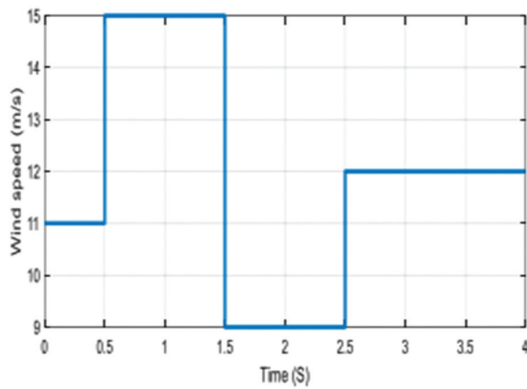
Fig. 13. Wind speed profile

Fig. 14 and 15 illustrate the proposed management and control strategy's performances under variable wind speeds.
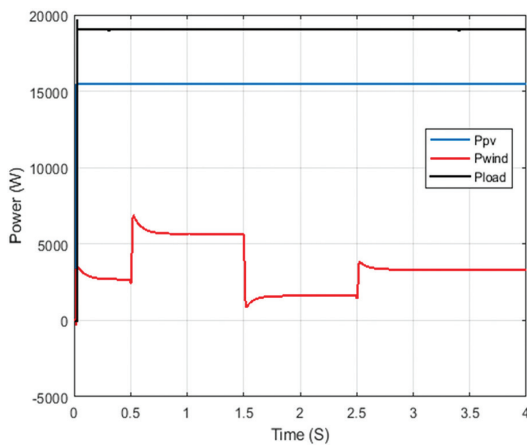
Fig. 14. Simulation of P_{pv}, P_{wind} and P_{load} with variable wind speed.
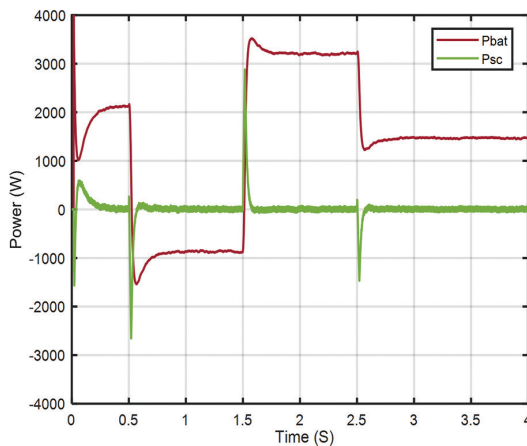
Fig. 15. Simulation of P_{bat}, and P_{sc} with variable wind speed

The wind power supplies about 3 kW from (0 s to 1s), the PV panel provides 15 kW, and the battery delivers the rest of the power needed by the load. Likewise, the battery power follows the wind power variations. When there is insufficient electricity, the battery discharges and provides the required energy. Alternatively, the battery is in charging mode and stores any excess power from several sources when there is a surplus.

Case: 3 Variable load with a constant solar irradiation and constant wind speed.

Fig. 16 shows the load profile considered in this simulation with a constant solar irradiance and wind speed.
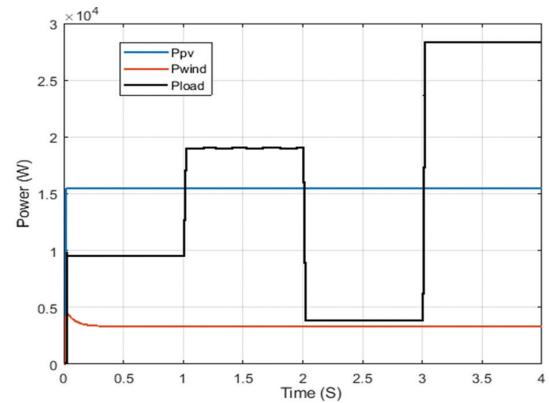
Fig. 16. Simulation of P_{pv}, P_{wind} and P_{load} under variable load.

The solar irradiance is set to 400 W/m2, where the photovoltaic cell power is equal to P_pv=16 kW, and the wind speed is 14 m/s, where the wind power is P_wind=6 kW. Similarly, the battery power follows the load variations. When there is insufficient electricity, the battery discharges and supplies the needed power. Alternatively, the battery is in charging mode and stores extra multi-source generation when there is an excess of power, as shown in Fig. 16 and 17.
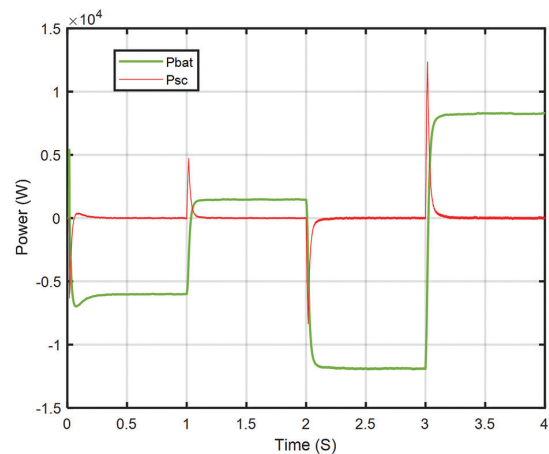
Fig. 17. Simulation of P_{bat}, and P_{sc} under variable load

Figure 18 illustrates the SoC of the supercapacitor variation under variable load. As it can be seen, there is a similarity between this profile and the profile of

supercapacitor power variation, because the supercapacitor's SoC follows the latter's power variation.
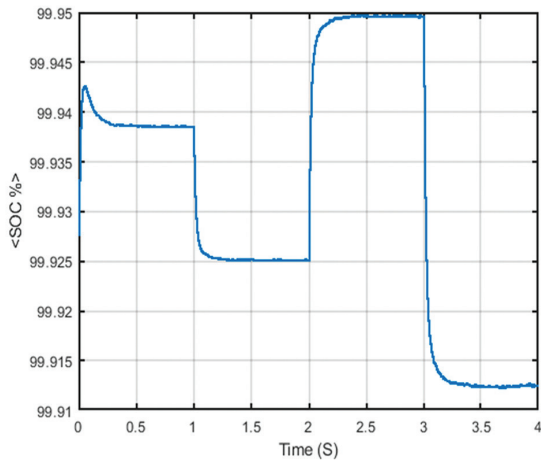
Fig. 18. Simulation of SoC_{sc}, under variable load

This control strategy also shows its performance by keeping the DC bus voltage closer to its reference value V_{dc}=400 V, as shown in Fig. 18. At (t=2 s), the load decreases from 20 kW to 4 kW. It can be observed on the zoomed-in section of the waveform in Fig. 19 that the DC bus voltage remains stable, this is on one hand.

On the other hand, Fig. 20 shows that the DC bus voltage is unstable and follows the fluctuations of the load or the different sources.
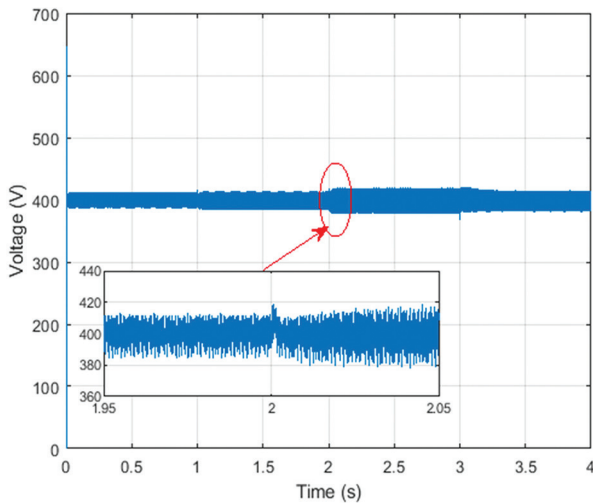
Fig. 19. Simulation of V_{dc} with power management, under variable load

Based on the three scenarios considered in this simulation study, the results of this study indicate that the batteries and supercapacitors can respond properly to the fluctuations of the electrical load demand. The SCs quickly provide or absorb peak powers in response to the load demands, to compensate the slow batteries' delay relatively. The current stress level on batteries is significantly reduced. The DC bus voltage is successfully maintained constant at 400 V, as required by the control and management strategy.
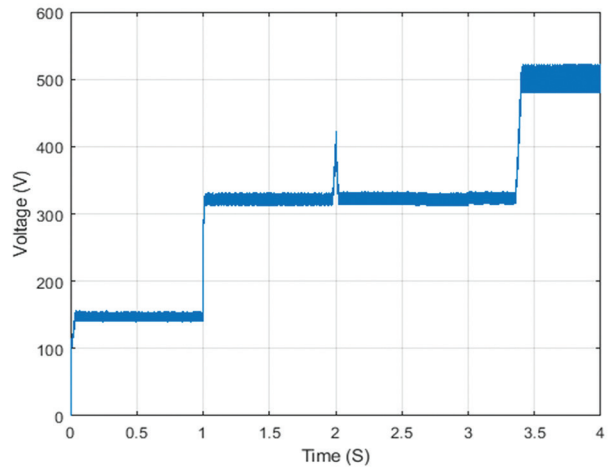
Fig. 20. Simulation of V_{dc} without power management, under variable load

5. CONCLUSION

The primary objective of the current study was to develop and evaluate a control strategy based on the regulation of the low-frequency power components of multisource generating systems and the load imbalance. Detailed modeling of the system's main components, such as photovoltaic and wind power, has been presented. Then, the proposed control strategy was detailed and tested. The results of this investigation, through the three simulation scenarios, prove the validity and goals of the control strategy: reducing of battery charge/discharge rates, improvement of voltage regulation, and the electric current causing lower stress levels on the battery, which increases the battery life. Future work can be focused on testing experimentally these microgrid performances under partial shading conditions.

6. APPENDIX

Table 2. System parameters used in the simulation study

Parameters	Values
PV array	
Open circuit voltage (V_{pv})	21 V
Short circuit current (V_{pv})	8 A
Number of Parallel strings (N_p)	20
Number of Series-connected modules per string (N_s)	16
Maximum Power (W)	120.7
Voltage at maximum power point Vmp (V)	17
Current at maximum power point Imp (A)	7.1
Wind energy system	
Stator phase resistance R_s (Ω)	2.875
Armature inductance (H)	0.000835
Flux linkage (Wb)	0.175
Number of pole pairs	4
Electrical power generator (kW)	6

Battery specifications	
Type	Lithium-Ion
Ah capacity	45
Terminal voltage (V_{bat})	12
Number of batteries in series	30
SC specifications	
Terminal voltage (V_{sc})	50
Capacitance (C_{sc})	25 F
Number of SCs in series	4
Converters parameters	
L_{pv}	0.352 mH
C_{pv}	100 µF
L_{bat}	0.3 mH
L_{sc}	0.355 mH
C_{dc}	7000 µF
L_f	5 mH
C_f	10 µF
PI controllers parameters	
K_{p_v}	1.477
K_{Pbat}	3077
K_{psc}	0.043
K_{i_v}	0.65
K_{ibat}	0.45
K_{isc}	100
DC and AC grid parameters	
V_{dc}	400 V
V_{ac}	220 V
f	50 Hz

PI	Proportional integrator	G_r	the solar insulation (W/m2)
N_p	Parallels modules	V_{ESS}	The voltage of the electrical energy storage (V)
N_s	series modules	V_{dc}	DC bus voltage (V)
C	DC bus capacitor (F)	P_{wid}	The wind power generator
R	The load resistance (Ω)	L_{pv}	The DC-DC converter inductance of the PV (H)
D_b	the duty ratio of the control of the DC/DC converter of the battery	L_b	The DC-DC converter inductance of the batteries (H)
SC	supercapacitor	L_{sc}	The DC-DC converter inductance of the supercapacitor (H)
D_{sc}	the duty ratio of the control of the DC/DC converter of the SC	I_{load}	The load current (A)
I_{dc_ref}	The DC bus current reference (A)	V_{dc_ref}	The DC bus reference voltage (V)
I_{sc_ref}	The SC current reference (A)	$K_{p\text{-}sc}$	The proportional factor of the SC corrector
I_{bat_ref}	The batteries current reference (A)	$K_{p\text{-}bat}$	The proportional factor of the battery corrector
V_{sc}	The supercapacitor voltage (V)	$K_{i\text{-}sc}$	The integrator factor of the SC corrector
V_{bat}	The battery voltage (V)	$K_{i\text{-}bat}$	The integrator factor of the battery corrector
I_{sc}	The SC current (A)	$K_{p\text{-}DC}$	The proportional factor of the DC bus corrector
I_{bat}	The battery current (A)	$K_{i\text{-}DC}$	The integrator factor of the DC bus corrector
PID	Proportional integrator derivator	P_{sc}	The SC power
P_{bat}	batteries power	P_{pv}	PV power
P_{load}	load power		

7. NOMENCLATURE

EES	electrical energy storage	R_s	series resistance (Ω)
$HEES$	hybrid electrical energy storage	R_p	parallel resistance (Ω)
SC	supercapacitor	I	solar cell current (A)
$PMSG$	permanent magnet synchronous generator	I_{ph}	Photocurrent (A)
P_m	captured wind power	I_s	cell saturation of dark current (A)
ρ	the air density (Kg/m3)	I_D	The diode current (A)
R	the radius of the rotor blade (m)	V_{pv}	solar cell voltage (V)
V_w	wind speed(m/s)	q	the electron charge (C)
C_p	the power coefficient	k	the Boltzman's constant (J/K)
PMS	power management strategy	T_c	the cell's working temperature
PV	photovoltaic	A	the ideality factor
DC	Direct current	I_p	parallel current (A)
$MPPT$	maximum power point tracking	T_{ref}	the cell's reference temperature (°C)

8. REFERENCES:

[1] K. C. Divya, J. Ostergaard, "Battery energy storage technology for power systems — An overview", Electric Power Systems Research, Vol. 79, 2014, pp. 511-520.

[2] T. Rout, M. K. Maharana, A. Chowdhury, S. Samal, "A Comparative study of Stand-alone Photo-Voltaic System with Battery storage system and Battery Supercapacitor storage system", Proceedings of the 4th International Conference on Electrical Energy Systems, Chennai, India, 7-9 February 2018, pp. 77-81.

[3] Y. Zhang, Z. Jiang, X. Yu, "Control Strategies for Battery / Supercapacitor Hybrid Energy Storage Systems", Proceedings of the IEEE Energy 2030 Conference, Atlanta, GA, USA, 17-18 November 2008, pp. 5-10.

[4] A. Ferrara, C. Hametner, "Impact of Energy Management Strategies on Hydrogen Consumption and Start-Up/Shut-Down Cycles in Fuel Cell-Ultracapacitor-Battery Vehicles", IEEE Transactions on Vehicular Technology, Vol. 71, No. 6, 2022, pp. 5692-5703.

[5] M. O. Qays, Y. Buswig, M. L. Hossain, A. Abu-Siada, "Recent progress and future trends on the state of charge estimation methods to improve battery-storage efficiency: A review", CSEE Journal of Power and Energy Systems, Vol. 8, No. 1, 2022.

[6] S. A. Ghorashi, K Abadi, S. I. Habibi, T. Khalili, A. Bidram, "A Model Predictive Control Strategy for Performance Improvement of Hybrid Energy Storage Systems in DC Microgrids", IEEE Access, Vol. 10, 2022, pp. 25400-25421.

[7] S. A. Ghorashi, K Abadi, A. Bidram, "A distributed rule-based power management strategy in a photovoltaic/hybrid energy storage based on an active compensation filtering technique", IET Renewable Power Generation, Vol. 15, No. 15, 2021, pp. 3688-3703.

[8] M. Robayo, M. Mueller, S. Sharkh, M. Abusara, "Assessment of supercapacitor performance in a hybrid energy storage system with an EMS based on the discrete wavelet transform", Journal of Energy Storage, Vol. 57, 2023, p. 106200.

[9] N. M. Ismail, M. K. Mishra, "A multi-objective control scheme of a voltage source converter with battery–supercapacitor energy storage system used for power quality improvement", International Journal of Electrical Power & Energy Systems, Vol. 142A, 2022, p. 108253.

[10] S, Xie, X, Hu, S, Qi, K, Lang, "An artificial neural network-enhanced energy management strategy for plug-in hybrid electric vehicles", Energy, Vol. 163, 2018, pp. 837-848.

[11] P. Mohan R., R. S. Sreelekshmi, M. G. Nair, "A Neural Network Based Hybrid Energy Storage System Connected to a DC Standalone PV System", Proceedings of the International Virtual Conference on Power Engineering Computing and Control: Developments in Electric Vehicles and Energy Sector for Sustainable Future, Chennai, India, 2022, pp. 1-5.

[12] A. M. Abomazid, N. A. El-Taweel, H. E. Z. Farag, "Optimal Energy Management of Hydrogen Energy Facility Using Integrated Battery Energy Storage and Solar Photovoltaic Systems", IEEE Transactions on Sustainable Energy, Vol. 13, No. 3, 2022, pp. 1457-1468.

[13] M. Faisal, M. A. Hannan, P. J. Ker, K. M. Muttaqi, "Genetic Algorithm based Fuzzy Logic Controller for Optimal Charging-Discharging of Energy Storage in Microgrid applications", Proceedings of the IEEE Industry Applications Society Annual Meeting, Detroit, MI, USA, 2022, pp. 1-9.

[14] K. R. Naik, B. Rajpathak, A. Mitra, M. Kolhe, "Adaptive Energy Management Strategy for Optimal Power Flow Control of Hybrid DC Microgrid", Proceedings of the 5th International Conference on Smart and Sustainable Technologies, Split, Croatia, 2020, pp. 1-6.

[15] A. Bharatee, P. K. Ray, A. Ghosh, "A Power Management Scheme for Grid-connected PV Integrated with Hybrid Energy Storage System", Journal of Modern Power Systems and Clean Energy, Vol. 10, No. 4, 2022, pp. 954-963, July 2022.

[16] S. A. Ghorashi, K Abadi, A. Bidram, "Effective utilization of grid-forming cloud hybrid energy storage systems in islanded clustered dc nano-grids for improving transient voltage quality and battery lifetime", IET Renewable Power Generation, Vol. 17, No. 8, 2023, pp. 1836-1856.

[17] H. Guentri, T. Allaoui, M. Mekki, M. Denai, "Power management and control of a photovoltaic system with hybrid battery-supercapacitor energy storage based on heuristics methods", Journal of Energy Storage, Vol. 39, 2021, p. 102578.

[18] B. Peng, X. Ma, X. Ma, C. Tian, "Fuzzy-based coordinated control and parameter correction strategy for speed controller of PMSG wind turbine in frequency response", Energy Reports, Vol. 9, No. 3, 2023, pp. 558-566.

[19] K. Palanimuthu, G. Mayilsamy, S. R. Lee, S. Y. Jung, Y. H. Joo, "Comparative analysis of maximum power extraction and control methods between PMSG and PMVG-based wind turbine systems", Energy Reports, Vol. 143, 2022, p. 108475.

[20] Y. Zhu, Z. Wang, X. Guo, Z. Wei, "An improved kinetic energy control strategy for power smooth-

ing of PMSG-WECS based on low pass filter and fuzzy logic controller", Electric Power Systems Research, Vol. 214A, 2023, p. 108816.

[21] Y. Belkhier, A. Achour, N. Ullah, R. N. Shaw, S. Chowdhury, K. Techato, "Energy-based fuzzy supervisory non integer control for performance improvement of PMSG-Based marine energy system under swell effect and parameter uncertainties", Renewable Energy, Vol. 186, 2022, pp. 457-468.

[22] G. Liu, T. Li, J. Su, "Photovoltaic fault diagnosis method based on BP neural network and rule-based control chart", Proceedings of the China International Conference on Electricity Distribution, Changsha, China, 2022, pp. 579-583.

[23] F. Bradaschia, M. C. Cavalcanti, A. J. do Nascimento, E. A. da Silva, G. M. de Souza Azevedo, "Parameter Identification for PV Modules Based on an Environment-Dependent Double-Diode Model", IEEE Journal of Photovoltaics, Vol. 9, No. 5, 2019, pp. 1388-1397.

[24] B. Guddanti, J. R. Orrego, R. Roychowdhury, M. S. Illindala, "Sensitivity Analysis Based Identification of Key Parameters in the Dynamic Model of a Utility-Scale Solar PV Plant", IEEE Transactions on Power Systems, Vol. 37, No. 2, 2022, pp. 1340-1350.

[25] P. V. H. Seger, P. X. Thivel, D. Riu, "A second life Li-ion battery ageing model with uncertainties: From cell to pack analysis", Journal of Power Sources, Vol. 541, 2022, p. 231663.

[26] K. Milić, S. M. Cvetićanin, N. Vukajlović, D. Milicević, M. Subotin, D. Pejić, "Fractional modeling and analytic solution of supercapacitor response", Proceedings of the IEEE PES Innovative Smart Grid Technologies Conference Europe, Novi Sad, Serbia, 2022, pp. 1-5.

[27] M. Keerthana, P. S. Manoharan, A. Ravi, "Design of Control Strategy for Battery-Supercapacitor Hybrid Storage System", Proceedings of the 7th International Conference on Communication and Electronics Systems, Coimbatore, India, 2022, pp. 798-803.